Simulation of stage I fatigue crack gowth in a polycrystal through coupled FEM and discrete dislocation dynamics

Graciela Bertolino, Véronique Doquet, Maxime Sauzay

Simulation of stage I fatigue crack growth in a polycrystal through coupled FEM and discrete dislocation dynamics

G. Bertolino[1,2], V. Doquet[1] & M. Sauzay[2]
[1]*L. M. S., CNRS, Ecole Polytechnique, France*
[2]*CEA, DEN-DMN-SRMA, France*

Abstract

An attempt to model the variability of short crack development in high-cycle fatigue is made by coupling finite element computations of the stresses ahead of a microcrack in a polycrystal with simulations of crack growth along slip planes based on discrete dislocations dynamics. The model predicts a large scatter in growth rates related to the crystallographic disorientations along the crack path. It also describes qualitatively the influence of the mean grain size and the fact that overloads may suppress the endurance limit by allowing arrested cracks to cross the grain boundaries.

1 Introduction

High-cycle fatigue is characterised by a large scatter in fatigue lives which reflects the scatter in mechanical conditions encountered by short cracks in the early stage of their development.

The stress distribution in a polycrystal can be very heterogeneous due to the elastic anisotropy of the grains. Moreover, the local texture influences both the ease of crack transfer beyond a grain boundary (GB) and the roughness of the crack. The effective crack driving force varies substantially with the local microstructure.

An attempt to model this variability is made by coupling finite element (FE) calculations of the stresses ahead of a microcrack in a polycrystal with simulations of crack growth along slip planes based on discrete dislocations

dynamics (DDD) [1]. Low amplitude reversed torsion tests are performed on 316LN stainless steel and microcracks development monitored to provide data for the model.

2 Experimental observations

The first reversed torsion test performed at ±120MPa on a specimen of 316L steel (mean grain size 50μm) was periodically interrupted for observations of the microcracks. The specimen was not broken at 10^6 cycles. However, one grain size-long crystallographic microcracks initiated close to the maximum shear planes (longitudinal and transverse) and blocked by a GB were already present at 70000 cycles (less than 7% of the fatigue life). Fretting debris came out from the microcracks flanks. Arrest periods of at least 20000 cycles due to the GBs were measured. Sometimes, cracks became arrested soon after crossing a GB. This case was often associated with a large deflection of the crack plane. For this stress level, the transition to Stage II propagation occurred most often when the cracks were three grain size-long. This transition did not always coincide with the transfer in a new grain but also occurred during transgranular propagation due to the activation of a secondary slip plane, 45° to the main crack direction. Early Stage II was still crystallographic, with a zig-zag crack path along two slip planes activated sequentially. Fatigue tests at different stress levels are in progress.

3 Principle of the simulations

Since high-cycle fatigue is considered, the computations of stress fields are performed in 3D elasticity, using CAST3M FE code. A mesh of the microcrack surrounded by a 30 grains circular multicrystal embedded in a homogeneous medium is built (Figure 1). The homogeneous medium constitutes a square plate on which borders global loading is applied. Each grain contains at least 20 quadratic elements. The mesh is refined in the grains containing the crack tip where the smallest elements are 0.1μm wide, so as to capture the associated stress concentration and gradient. The geometry of the grains, their size as well as their crystallographic orientations (denoted by the three Euler angles, ϕ_1, ϕ, ϕ_2) could be those determined by EBSD mapping of local texture during an experiment.

The elastic constants for austenite grains are taken as: C_{11}=197.5GPa, C_{12}=122GPa and C_{44}=125GPa. Those of the homogeneous medium surrounding the polycrystal are E=210GPa and ν=0.3.

Since Stage I crystallographic propagation in a FCC metal due to mixed mode I + II loading is modeled, the crack follows {111} planes and its front is supposed to be normal to a <-1 1 0> direction, so that the dislocations emitted at its tips have a pure edge character.

The mode I and mode II stress intensity factors (SIF), are determined as the limit of $\sqrt{2\pi x}.\sigma_{xx}$ and $\sqrt{2\pi x}.\sigma_{xy}$, respectively, as x goes to zero (where x denotes the abcissa in a coordinate system centered at the crack tip with its first axis

tangent to the local crack direction). Due to crack roughness and elastic interactions between neighbouring grains, some normal compressive stress can be induced along the crack flank even in the absence of any macroscopic compression. A condition of non interpenetration had been imposed (in a later development of the simulations, crack flanks friction will be taken into account).

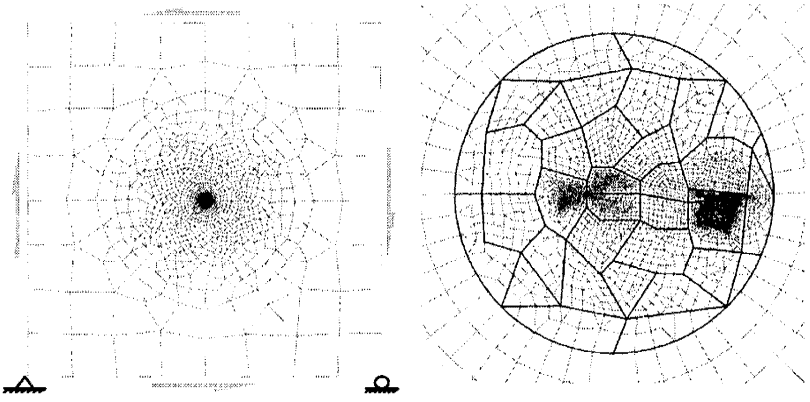

Figure 1: Mesh of the circular multicrystal embedded in a homogeneous medium.

Since cyclic loading is considered, the SIFs are computed under maximum and minimum global stresses as well as the distribution of σ_{xy} in the crack plane, between the crack tip and the closest GB. Even under fully reversed global loading, the loading path undergone by the crack is not symmetrical but is constituted with one segment in mixed mode I+II and one segment in pure shear. The mode I component is considered to assist crystallographic crack propagation when it is present (through its influence on dislocation emission as explained below, or an attenuation of crack flanks friction, not yet taken into account) but not to drive it. In other words, only coplanar slip is activated by the mode II component, mode I opening being purely elastic. The values of K_{Imax}, K_{IImax} and K_{IImin} as well as the shear stress profile $\sigma_{xy}(x)$ ahead of the crack tip computed that way are used as input for simulations of crack tip plasticity based on discrete dislocation dynamics.

The expression of the stress field generated by a dislocation in an anisotropic elastic medium can be found (see for example Okasaki et al [2]) after the resolution of a sextic equation whose coefficients depend on the elastic constants, the slip plane and the slip direction. For an infinite edge dislocation lying along the (1 -1 2) direction (that is: parallel to the crack front) with a Burgers vector b = a/2 (1 1 0) in a FCC crystal, the in plane shear component is of the form: $Ab/2\pi x$ where A is a constant which depends on the roots of the sextic equation. A reduces to $\mu/(1-\nu)$ for an isotropic elastic medium. In the present case (anisotropic) A = 107GPa.

The critical mode II stress intensity factor for the emission of a coplanar edge dislocation from the crack tip is calculated as a function of the mode mixity parameter Ψ:

$$K_{II}^{nucl}=\sqrt{2A[\gamma_{us}^{r}-\alpha(\gamma_{us}^{u}-\gamma_{us}^{r})(\frac{\pi}{2}-\psi)]} \quad \text{where} \quad \psi=Arctan(\frac{K_{II}}{K_I}) \qquad (1)$$

where α, γ_{us}^{u} and γ_{us}^{r} are materials parameters. Since $\gamma_{us}^{u} > \gamma_{us}^{r}$, eqn (1) predicts a lower threshold stress intensity factor for dislocation nucleation when Ψ decreases, that is, when an opening stress is present (for more details, see [3])
The shear stress on the i^{th} dislocation at abscisa x_i zone is evaluated as:

$$\tau_i=\sigma_{xy}(x_i)-\frac{Ab_i}{4\pi x_i}-\sum_{j\neq i}\frac{Ab_j}{2\pi}\sqrt{\frac{x_j}{x_i}}.\frac{1}{x_j-x_i} \qquad (2)$$

in which the three terms represent respectively the shear stress distribution ahead of the crack computed by FE, the image stress (the crack flanks are free surfaces) and the stress field of other dislocations. Strictly, this equation (as well as eqn (4) below) is valid for a semi infinite crack. For a crack of finite length, different expressions have to be used (see for example Tanaka and Akinawa [4]). But in the present case, the free path of dislocations is limited by GBs and it has been checked that the difference in predicted crack growth rates considering finite length or not is small.

The velocity of each dislocation is calculated (noting the positive part of a number by brackets) as:

$$v_i=v_0.sign(b_i.\tau_i)\left\langle|\tau_i|-\tau_f\right\rangle^m \qquad (3)$$

where τ_f is the lattice resistance to dislocation glide, v_0 and m two constants (without any influence for the frequencies used in classical fatigue tests).

The new position of each dislocation is then deduced, and annihilation criteria checked: if a dislocation comes close enough to the crack tip or to a dislocation of opposite sign, it is removed from the simulation.

The real mode II stress intensity factor, allowance made for crack tip shielding by the dislocation stress field is then evaluated as:

$$K_{II}^{tip}=K_{II}-\sum_{i=1}^{n}\frac{Ab_i}{\sqrt{2\pi x_i}} \qquad (4)$$

The dislocation emission criterion:

$$K_{II}^{tip} \leq -K_{II}^{nucl} \quad \text{or} \quad K_{II}^{tip} \geq K_{II}^{nucl} \qquad (5)$$

is checked to decide whether a negative or positive dislocation can be emitted.

This sequence is repeated until the second cycle is completed. Then, the crack growth rate per cycle is computed. The crack is considered to grow by one Burgers vector each time a pair of positive-negative dislocation has been emitted or when a dislocation returns to the crack tip since both events correspond to some cyclic plastic flow at the crack tip and should thus contribute to its growth.

Grain boundaries are considered as impenetrable obstacles for the dislocations emitted by the crack. This implies crack deceleration and arrest, unless a source is activated in the next grain, which, after an incubation period could initiate a crack that would link with the arrested one, thus allowing further propagation.

The stress concentration due to the pile up, likely to promote source activation in the next grain is estimated as follows. Head [5] has shown that a dislocation of Burgers vector b in a medium of shear modulus μ_1 close and parallel to an interface with a different elastic medium, of modulus μ_2, generates in this medium the same stress field as a dislocation of Burgers vector $2\mu_1 b/(\mu_1+\mu_2)$. The in-plane shear moduli of the grain containing the crack tip and that of his neighbour are computed in the coordinate system tangent to the crack tip, and the stress field in the next grain due to the dislocations piled up on the GB is approximated with Head's formula.

This stress field is added to the elastic stress field computed by FE and the resolved shear stresses on the potential slip systems of the next grain which do not imply a twist of the crack plane (or, in other words, whose normal belongs to the free surface) are computed at a distance of 1μm from the GB.

There are two reasons for this condition on the potential slip systems: first, the experimental work of Zhai et al [6] has shown that the path most likely to be followed by the crack is generally the one which minimises its twist deflection and second, the 2D nature of the model would not allow the description of 3D tortuosity of the crack path.

If one of the computed resolved shear stresses τ_{res} exceeds a critical value, τ_s, a source is considered to be activated and the number of cycles, N_{inc}, for crack initiation due to the activity of this source followed by linking with the arrested crack is estimated to be elapsed when,

$$\int_1^{N_{inc}} C\left(\tau_{res}(N)-\tau_s\right)^n dN=1 \qquad (6)$$

where C and n are constants to be determined from experimental data on short cracks kinetics. Eqn (6) was inspired from the incubation model of Morris et al [7]. Ludwig et al [8] also report arrested microcracks in spite of a well visible plastic zone in the next grain. This means that the transfer of a crack tip beyond the boundary does not coincide with the activation of a slip system but requires a maturation time. When condition (6) is verified, a new mesh with a 1μm long branch crack in the next grain is generated and the whole process starts again.

The numerical values of the materials parameters used for the simulations are gathered in Table 1. With these values, the dislocation emission threshold in pure shear is 0.55MPa$\sqrt{m}$. Unless specified, the applied shear stress is ±130MPa and the mean grain size 50μm. Table 2 defines the simulated crack paths (the angle

denotes the inclination of the crack plane relative to the horizontal maximum shear plane). For sake of simplicity, one tip of the crack is arrested by an impenetrable GB (thanks to an appropriate choice of Euler angles in the neighbouring grain) so that only one tip has to be monitored.

Table 1: Parameters used in the simulations.

γ_{us}^{u} [J.m^{-2}]	γ_{us}^{r} [J.m^{-2}]	α	τ_f [MPa]	τ_s [MPa]	C [MPa$^{1/n}$]	n
1.41	1.64	1	58	96	5.e-10	2

Table 2: Definition of the crack paths.

	grain 1	grain 2	grain 3	grain 4
path 1	0°	-20°	+10°	-10°
path 2	0°	-35°	20°	/
path 3	0°	-45°	/	/
path 4	0°	-10°	+5°	-10°

4 Results from the simulations

The evolution of the maximum computed SIFs with microcracks length (projected on the maximum shear plane) for crack paths n°1, 2 and 4 are plotted on figure 2. The evolution of K_{II} obtained using a uniform stress approximation ($K_{II}=\tau_{app}.\sqrt{\pi a}$) is also reported for comparison.

It appears that this approximation systematically overestimates K_{II} because the most favourable grain orientation for crack initiation corresponds to a shear modulus which is only 83% of the average modulus on the one side, and the above-mentioned approximation is for a straight crack, whereas roughness shields the crack tip singularity, on the other side. Furthermore, K_{II} is highly variable from one microcrack to the other, depending on their paths. It does not systematically increase with the crack length but it may exhibit a sudden drop due to tilting at a GB (and in the case of path n°2, K_{II} falls below the emission threshold just after entering grain n°3 and the crack thus gets arrested). The mode mixity also shows abrupt variations and it may be surprisingly high for cracks which are not very far away from the nominally pure shear plane.

The computed arrest time at the first GB increases with the tilt angle of the crack plane in the next grain as illustrated by Figure 3. Since in the orientation most favourable to initiation the microcrack is loaded in pure shear, the activation of a slip system at 45° -a principal plane- is impossible and in that case, the crack gets arrested. Note that it might be different in presence of a mode I component.

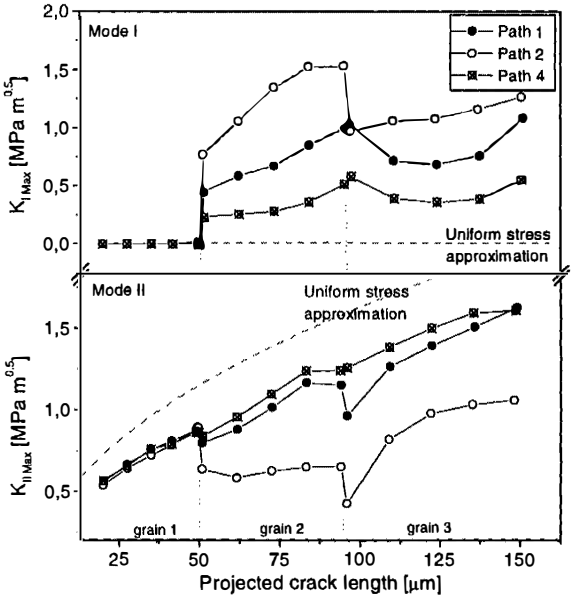

Figure 2: Evolution of the maximum computed SIFs with projected microcracks length for crack paths n°1, 2 and 4.

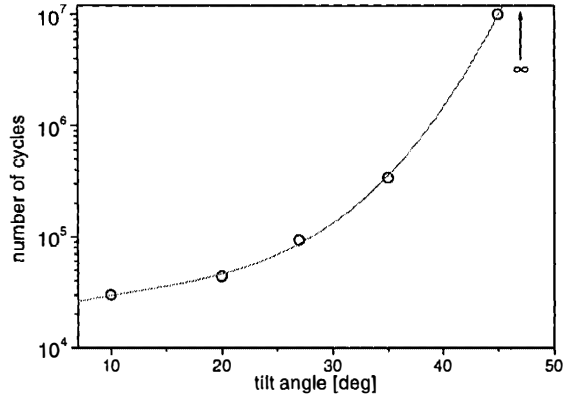

Figure 3: Evolution of the computed arrest time at the first G.B. with the tilt angle of the crack plane.

Figure 4 compares the evolution of the projected lengths for the different crack paths. For a given path, the incubation period due to GBs is smaller and smaller as the crack grows. This might seem surprising for path n°1 (arrest at the

first GB: 43043 cycles for a tilt of 20°, but only 39464 cycles at the second GB whereas the relative tilt is 30° and K_{II} is smaller than in the first grain, see Figure 3). This is due to the contribution of the mode I component which is quite high in the second grain.

The influence of the stress range is illustrated on Figure 5 that mimics a Wohlers plot. The number of cycles needed to develop a crack, twice the mean grain size in length varies a lot with the crack path. Note that the scatter in lives increases as the stress range decreases (for ±140MPa, 10 times more cycles are needed to cross the first GB for crack path n°2 than for n°4, whereas for ±110MPa, the ratio is 15). This is consistent with experimental observations.

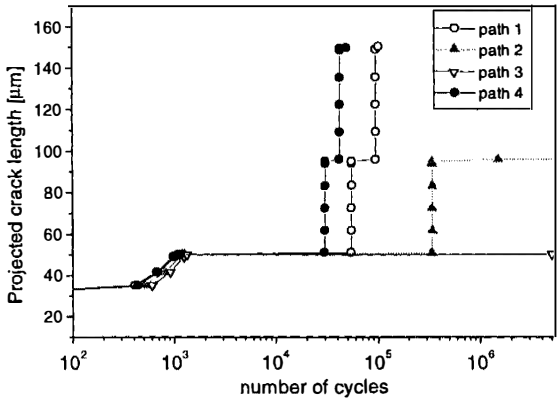

Figure 4: Evolution of the projected lengths for the different crack paths.

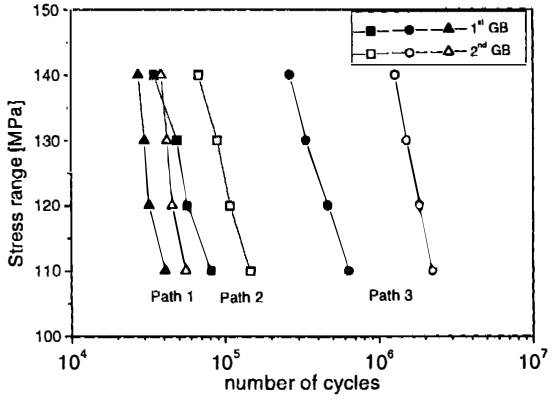

Figure 5: Influence of the stress range.

Figure 6 shows how the number of cycles needed for a crack to enter the second grain varies with the mean grain size. First it can be noticed that in accordance with experimental observations, most of the life is spent in arrest periods and very little in transgranular propagation. Second, as the mean grain size increases, the stress concentration in the next grain gets higher, due to an increased SIF, and more space to pileup emitted dislocations, so that crack transfer becomes easier and the endurance is reduced, consistently with experimental results.

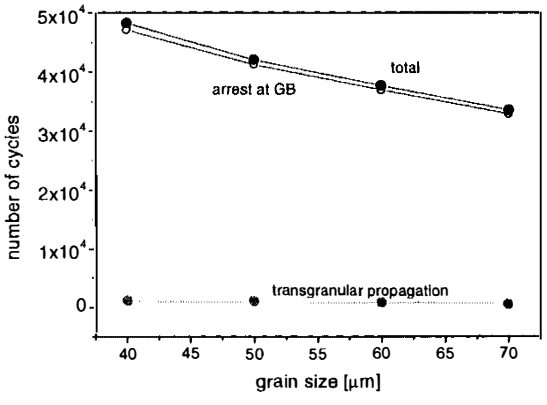

Figure 6: Variation of the number of cycles needed for a crack to enter the second grain with the mean grain size.

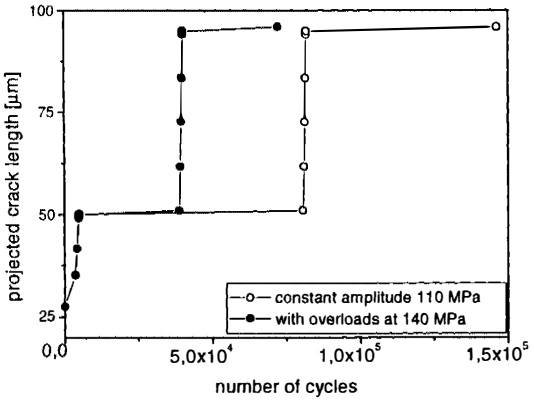

Figure 7: Influence of a few (45) overload cycles at ±140 MPa on microcrack growth under ±110 MPa.

Many experimental data in the literature show that a few overloads may remove the endurance limit because these cycles enable arrested microcracks to cross G.Bs. The present model reproduces this fact, as illustrated by Figure 7.

For a normal stress range of ±110MPa, fourty five overload cycles at ±140MPa applied when the crack tip is close to the first and second GB reduce by a factor of two the number of cycles needed to grow the crack to the third grain.

5 Conclusions

Crystallographic propagation of fatigue cracks in a polycrystal was modelled using local stresses computed by FE as input for discrete dislocation dynamics simulations. The simulations reproduce the scatter in microcracks growth rates associated with various local textures and an increased scatter for small loading ranges. Longer fatigue lives are predicted for small grain size materials. The decrease in the arrest periods at GBs as a crack develops is reproduced. The fact that overloads may suppress the endurance limit by unlocking microcracks arrested at GBs is also qualitatively described by the model.

Acknowledgements

The authors acknowledge the support from CEA, CNRS and EDF (through CPR SMIRN).

References

[1] Doquet, V.,Micromechanical simulations of microstructure-sensitive Stage I fatigue crack growth, *Fat. Fract. Eng. Mat. Struct.* **22**, pp 215-223, 1999.

[2] Okazaki, M, Analysis of crack tip sliding displacement in anisotropic elastic media and its application to Stage I fatigue crack growth, *Met.Trans.*, **22A**, pp 479-487, 1991.

[3] Sun, Y., Beltz, G.E., Rice, J.R., Estimates from atomic models of tension-shear coupling in dislocation nucleation from a crack tip, *Mat. Sci. Eng.*, A170, pp 67-85m 1993.

[4] Tanaka, K., Akinawa,Y.,Mechanics of small fatigue crack propagation, *Short fatigue cracks, mechanics and mechanisms*, pp 59-71, Ritchie, Ravichandran and Murakami eds, Elsevier 1998.

[5] Head, A.K.,The interaction of dislocations and boundaries, *Phil. Mag.*,**44 n° 348**, pp 92-94, 1952.

[6] Zhai T., Wilkinson A., Martin J.W., A crystallographic mechanism for fatigue crack propagation through grain boundaries, *Acta Mater.*, **48**, pp 4917-27, 2000.

[7] Morris, W.L., James, M.R., Buck, O.,Growth rate models for short surface cracks in Al 2219-T851, *Met. Trans.* **12A**, pp 57-64 , 1981.

[8] Ludwig W., Buffière J.Y., Savelli S., Cloetens P., Study of the interaction of a short fatigue crack with grain boundaries in a cast aluminium alloy using X-ray microtomography, to appear in *Acta Materialia*, **51 N°3**, 2003.